OUKA
The University of Osaka
Institutional Knowledge Archive

Title	Non-invasive quantitative assessment of kidney injury using near-infrared autofluorescence imaging
Author(s)	Matsumoto, Ayumi; Matsui, Isao; Fushiki, Hiroshi et al.
Citation	Kidney International. 2026, 110(3), p. 625-642
Version Type	VoR
URL	https://hdl.handle.net/11094/106744
rights	This article is licensed under a Creative Commons Attribution 4.0 International License.
Note	

The University of Osaka Institutional Knowledge Archive : OUKA

https://ir.library.osaka-u.ac.jp/

The University of Osaka

Non-invasive quantitative assessment of kidney injury using near-infrared autofluorescence imaging

see commentary on page 526

OPEN

Ayumi Matsumoto[1,7], Isao Matsui[1,2,7], Hiroshi Fushiki[3], Yasuo Kusunoki[4], Natsune Tamai[1], Hiroki Okushima[1], Atsuhiro Imai[1], Motoko Shimada[1], Takehito Harimoto[1], Taigo Kato[5], Koji Hatano[5], Yoichi Kakuta[5], Atsunari Kawashima[5], Shun-Ichiro Ogura[6], Norio Nonomura[5], Kazunori Inoue[1] and Yoshitaka Isaka[1]

[1]Department of Nephrology, Graduate School of Medicine, The University of Osaka, Osaka, Japan; [2]Transdimensional Life Imaging Division, Institute for Open and Transdisciplinary Research Initiatives, The University of Osaka, Osaka, Japan; [3]Bioimaging Lab, Translational Science Laboratories, Drug Discovery Research, Astellas Pharma Inc., Ibaraki, Japan; [4]Department of Nephrology, Toyonaka Municipal Hospital, Osaka, Japan; [5]Department of Urology, Graduate School of Medicine, The University of Osaka, Osaka, Japan; and [6]Department of Life Science and Technology, School of Life Science and Technology, Institute of Science Tokyo, Yokohama, Japan

Abstract

Introduction: Tubulointerstitial fibrosis represents the final common pathway to kidney failure, with tubular epithelial cell (TEC) injury playing a critical role. Current methods for assessing TEC injury rely on invasive biopsies or lack temporal resolution, limiting real-time monitoring of disease progression and therapeutic responses.

Methods: Near-infrared (NIR) autofluorescence was evaluated for non-invasive TEC injury assessment in three mouse models: unilateral ureteral obstruction (UUO; consistent tubulointerstitial injury), folic acid nephropathy (variable injury severity), and unilateral ischemia-reperfusion injury (IRI; acute tubular injury), without exogenous probes. Mechanistic studies used BALB/c-*Cpox*^{nct} mice, which harbor a spontaneous missense mutation reducing coproporphyrinogen oxidase activity, an enzyme that metabolizes coproporphyrinogen III in heme biosynthesis. Kidney slice cultures were treated with the mitochondrial complex III inhibitor antimycin A or the mitochondrial reactive oxygen species scavenger MitoTEMPO. Human kidney samples (non-cancerous region of nephrectomies) were examined *ex vivo*.

Results: NIR autofluorescence correlated with TEC injury, oxidative stress markers, and fibrosis across all three models. Spectroscopic analysis identified coproporphyrin III as the likely primary fluorophore. *Cpox* mRNA and CPOX protein were consistently reduced in injured kidneys. CPOX was expressed in proximal tubules and lost in damaged cells. BALB/c-*Cpox*^{nct} mice showed elevated baseline autofluorescence, which increased further after UUO, with HPLC confirming accumulation of the porphyrin metabolite coproporphyrin III. In kidney slice cultures, antimycin A reduced CPOX protein and enhanced autofluorescence; MitoTEMPO reversed both effects. To test whether autofluorescence can track therapeutic responses, finerenone (non-steroidal, mineralocorticoid receptor antagonist) was administered in UUO and bilateral IRI models; treated mice showed reduced autofluorescence that correlated with improved histology. In 34 human samples, autofluorescence correlated inversely with eGFR and positively with periodic acid-Schiff stain injury scores.

Conclusions: NIR autofluorescence enables non-invasive, real-time assessment of kidney injury without external agents. This approach has immediate applications for longitudinal monitoring in preclinical research demonstrating proof-of-concept for future development of clinically applicable imaging approaches.

Kidney International (2026) **110,** 625–642; https://doi.org/10.1016/j.kint.2026.05.016

KEYWORDS: biomarker; coproporphyrin; near-infrared autofluorescence; noninvasive imaging; tubular epithelial cell injury; tubulointerstitial fibrosis

© 2026 THE AUTHORS. Published by Elsevier Inc. on behalf of the International Society of Nephrology. This is an open access article under the CC BY license (http://creativecommons.org/licenses/by/4.0/).

Tubulointerstitial fibrosis is an important predictor of kidney survival.[1–3] Even when the initial injury does not directly target the renal tubules, the extent of tubulointerstitial fibrosis remains the most reliable indicator in chronic kidney disease.[4–8] Recent studies have revealed that tubular epithelial cell (TEC) damage is the central driver of this fibrotic process.[9–12] However, current approaches for assessing TEC injury have clear limitations. Kidney biopsy, the diagnostic gold standard, is invasive and provides only a single time point. Tubular injury biomarkers, such as kidney injury molecule-1 (KIM-1) and neutrophil gelatinase-

Correspondence: *Isao Matsui, Department of Nephrology, Graduate School of Medicine, The University of Osaka, 2-2 Yamadaoka, Suita, Osaka 565-0871, Japan. E-mail: matsui@kid.med.osaka-u.ac.jp*

[7]AM and IM contributed equally to this work.

Received 16 October 2025; revised 7 May 2026; accepted 21 May 2026; published online 18 June 2026

Translational Statement

Near-infrared autofluorescence, leveraging the optical window of biological tissues for deep penetration, enables noninvasive, real-time quantification of kidney injury without exogenous probes or genetic modifications. We demonstrate strong correlations between autofluorescence intensity and both histologic damage and oxidative stress markers across 3 distinct mouse models and human kidney samples. Mechanistically, reduced coproporphyrinogen oxidase activity in injured tubular epithelial cells likely leads to coproporphyrin III accumulation, providing the molecular basis for enhanced autofluorescence signals. This endogenous biomarker approach successfully detected therapeutic responses to finerenone treatment, demonstrating utility for monitoring treatment efficacy. The method's label-free nature, combined with validation in human tissues showing correlation with estimated glomerular filtration rate and injury severity, establishes proof of concept for clinical applications in monitoring kidney disease progression and therapeutic responses.

associated lipocalin, in serum or urine integrate signals from the whole organ but lack spatial resolution. Ultrasonographic and magnetic resonance imaging offer anatomic information but cannot quantify molecular-level damage. These limitations indicate the need for noninvasive methods that can assess TEC injury in real time with spatial resolution.

Fluorescence imaging has been explored to address these challenges. Fluorescence molecular tomography with Cy7-labeled collagen-binding adhesion protein 35 enables real-time monitoring of kidney fibrosis,[13] and nuclear factor-κB luciferase reporter mice allow visualization of inflammation.[14] Both approaches, however, depend on exogenous fluorophores or genetic modification, which restricts their use in routine experiments and precludes direct clinical translation. An imaging strategy that exploits endogenous tissue properties, without external probes or genetic engineering, would overcome these constraints.

Near-infrared (NIR) light is well suited for *in vivo* imaging because it falls within the optical window (650–950 nm) of biological tissues, where hemoglobin and water absorption is minimal and tissue penetration is greater than with visible light.[15–17] Biological tissues contain various endogenous fluorophores, including amino acids, nucleotides, and porphyrins, and porphyrins in particular emit in the long-wavelength region accessible to NIR detection.[18] We hypothesized that NIR excitation of endogenous fluorophores could visualize TEC injury without exogenous probes or genetic modification, enabling noninvasive, longitudinal monitoring in preclinical models.

To test this hypothesis, we used 3 mouse models with distinct injury mechanisms. The unilateral ureteral obstruction (UUO) model produces consistent and progressive injury with minimal variability and allowed us to establish the quantitative relationship between autofluorescence and injury severity. The folic acid–induced nephropathy model, which shows substantial interindividual variability, allowed us to test whether this relationship holds across a range of damage intensities. The unilateral ischemia-reperfusion injury (IRI) model extended validation to acute kidney injury. We further examined human kidney samples *ex vivo* to assess broader applicability. Our findings show that NIR autofluorescence enables noninvasive, quantitative assessment of TEC injury and provides mechanistic insight into its molecular origin.

METHODS

Animals and experimental models

All animal experiments were approved by the University of Osaka Animal Committee (approval number: 02-006-008) and conducted in accordance with the National Institutes of Health guideline. Male BALB/c mice (Japan SLC), aged 7 to 8 weeks, were used for the main experiments. For evaluation in dark-coated mice, male C57BL/6J mice, aged 7 to 8 weeks (Japan SLC), were used and subjected to UUO. Mice were housed in a specific pathogen-free facility (22 °C–24 °C, 12-hour light-dark cycle). They had *ad libitum* access to an AIN-93G diet (CLEA Japan) and water. For invasive procedures, mice were anesthetized by i.p. injection of medetomidine, midazolam, and butorphanol. Sample sizes were determined based on the 3R principles (replacement, reduction, and refinement). Cage arrangements were randomized to reduce confounding. Animals that exhibited fighting behavior were excluded from the study.

UUO was performed by exposing the kidney through flank incision. The ureter was ligated at 2 points using silk sutures and transected between the ligatures. The sham control group underwent identical surgical exposure without ureteral manipulation. Folic acid nephropathy was induced by i.p. injection of folic acid (200 mg/kg; Sigma-Aldrich) dissolved in 0.3 mol/l $NaHCO_3$. Unilateral IRI was performed by clamping the left renal pedicle for 25 minutes to induce warm renal ischemia. Bilateral IRI was performed by simultaneously clamping both renal pedicles for 15 minutes; the shorter ischemic time was used to avoid excessive mortality. BALB/c-coproporphyrinogen oxidase ($Cpox)^{nct}$ mice, a spontaneous *Cpox* gene mutant strain, were obtained from the RIKEN BioResource Research Center (number RBRC00422). The BALB/c-$Cpox^{nct}$ mice underwent UUO surgery and were analyzed on day 3.

For δ-aminolevulinic acid (δ-ALA) experiments, wild-type BALB/c mice on UUO day 3 received an i.p. injection of δ-ALA (300 mg/kg; FUJIFILM Wako) dissolved in saline. In the finerenone study, wild-type BALB/c mice were orally administered finerenone (10 mg/kg; MedChemExpress) or vehicle daily, starting 2 days before UUO or bilateral IRI

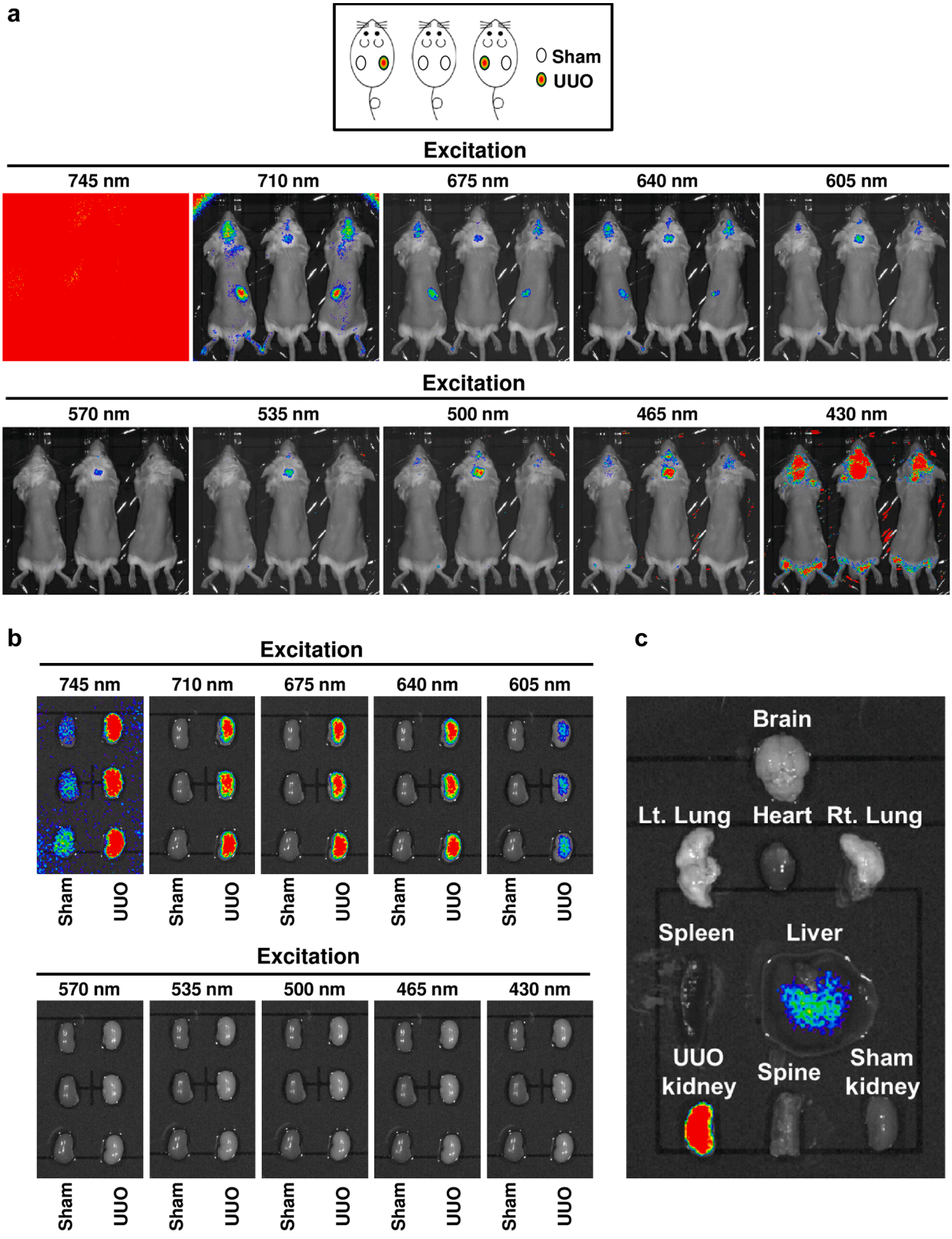


Figure 1 | Near-infrared autofluorescence detects kidney injury in the unilateral ureteral obstruction (UUO) model. (**a**) *In vivo* autofluorescence imaging of BALB/c mice 7 days after sham or UUO surgery. Images were acquired using an IVIS imaging system (PerkinElmer) with excitation filters ranging from 430 to 745 nm and an emission filter of 810 to 875 nm. Mice were epilated before imaging. Radiant efficiency range: 1.63E+6 to 2.40E+6 p/s/cm^2/sr per μW/cm^2. (**b**) *Ex vivo* autofluorescence of surgically removed kidneys on day 7 after UUO. Radiant efficiency range: 2.15E+6 to 3.50E+6 p/s/cm^2/sr per μW/cm^2. (**c**) Autofluorescence of various organs from UUO mice on day 7, imaged using parameters in (**b**). Representative of 3 independent experiments. Lt, left, Rt, right.

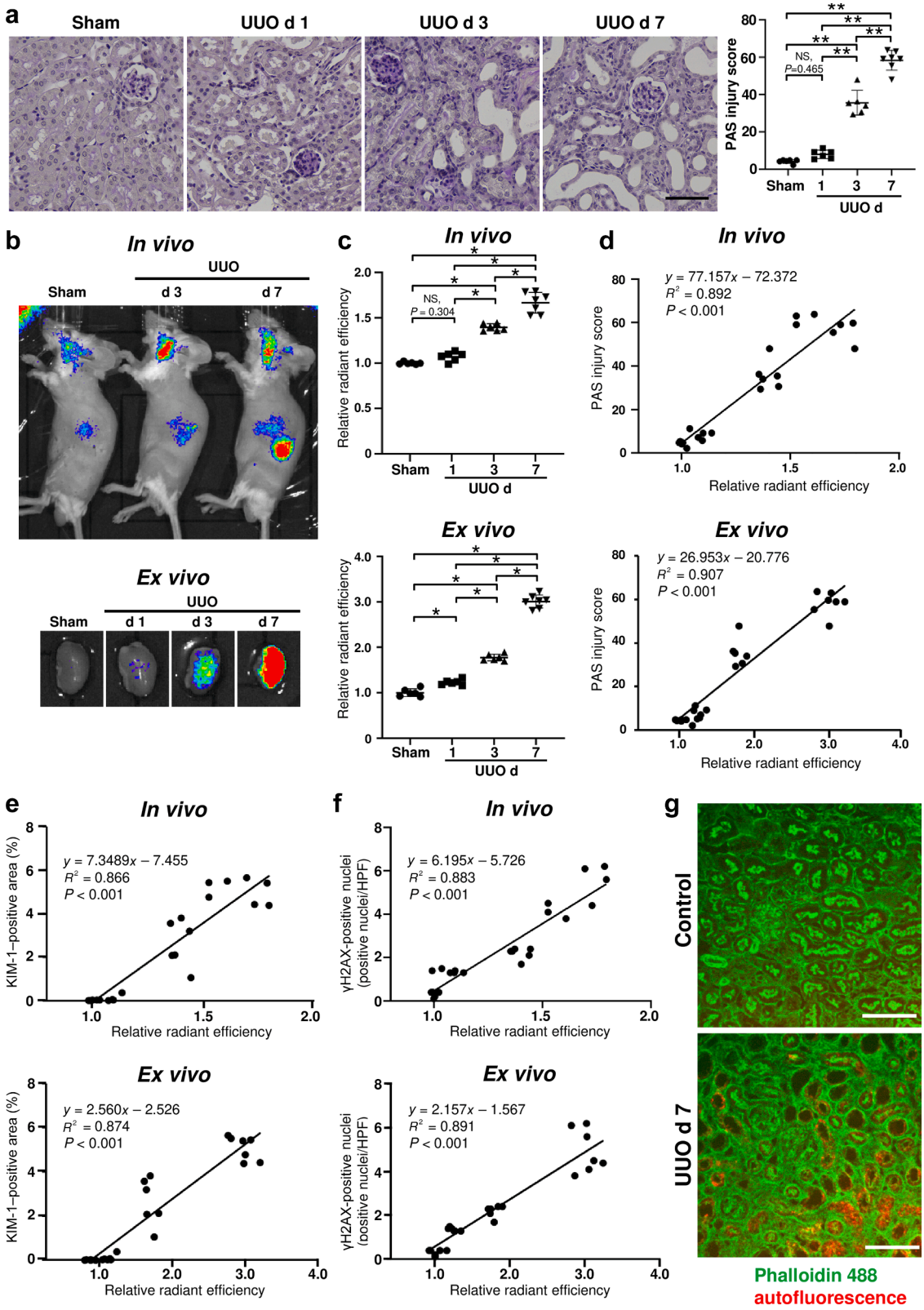


Figure 2 | Near-infrared autofluorescence correlates with tubular epithelial cell (TEC) injury severity in the unilateral ureteral obstruction (UUO) model. (**a**) Progressive TEC injury quantified by periodic acid–Schiff (PAS) staining. Representative images and quantification shown (n = 6–7 per time point; $^{**}P < 0.01$, Tukey-Kramer test; bar = 100 μm). (**b**) Representative *in vivo* and *ex vivo* autofluorescence images (excitation: 710 nm, emission: 810–875 nm) at indicated time points after UUO. (**c**) Quantified autofluorescence intensity normalized to sham controls (n = 6–7 per time point; $^{*}P < 0.05$, Tukey-Kramer test). (**d–f**) Correlations between autofluorescence and (**d**) PAS injury scores (n = 25), (**e**) kidney injury molecule (KIM)-1–positive areas (n = 25), and (**f**) Phosphorylated histone (continued)

surgery and continuing until sacrifice. Finerenone was prepared as a 20 mM stock solution in dimethylsulfoxide and suspended in 0.5% w/v methyl cellulose 400 (FUJIFILM Wako) for administration. For 4-hydroxy-2,2,6,6-tetramethylpiperidine-1-oxyl (TEMPOL) administration experiments, wild-type BALB/c mice underwent UUO or bilateral IRI on day 0 and received 4-hydroxy-TEMPO (176141, Sigma-Aldrich) in drinking water (1.0 mM) starting on day 5 until sacrifice on day 7.

Human kidney samples

Human kidney tissues were obtained from patients who underwent nephrectomy for malignant tumors at the University of Osaka Medical Hospital. Nontumor portions of kidney tissues were cut into pieces small enough to fit in a 1.5-ml tube and stored at −80 °C until analysis. For autofluorescence measurement, tissue pieces were thawed and imaged directly using the IVIS system (PerkinElmer) under the same conditions as *ex vivo* mouse kidney samples. The same samples were subsequently used for RNA extraction. Estimated glomerular filtration rate values were obtained from routine blood tests. Written informed consent for the use of the kidneys was obtained from all patients. The Ethics Committee of the University of Osaka Medical Hospital approved the study protocol (approval number: 14317-2). The study was conducted in accordance with the Declaration of Helsinki.

Kidney slice culture

Wild-type BALB/c mice on UUO day 3 were anesthetized and perfused with ice-cold phosphate-buffered saline. The UUO and contralateral kidneys were removed, kept on ice, and cut into 300-μm slices with a vibratome (Leica VT1000S). During slicing and the brief interval before transfer to culture, slices were held in ice-cold phosphate-buffered saline continuously bubbled with 96% O_2 from an oxygen concentrator. From each kidney, six 300-μm transverse sections through the central region containing both cortex and medulla were collected and assayed together as a single set. Slices were cultured at 37 °C in high-glucose Dulbecco's modified Eagle's medium (16971-55, Nacalai Tesque) containing 10% fetal calf serum and penicillin-streptomycin (15140122, Gibco), with 1.5 ml of medium per well of a 6-well plate. The plate was placed in a sealed chamber filled with 95% O_2 and 5% CO_2. To inhibit the mitochondrial electron transport chain, antimycin A (A8674, Sigma-Aldrich) was added at 5.0 μM, and slices were incubated for 8 hours. For mitochondrial reactive oxygen species scavenging experiments, δ-aminolevulinic acid (012-13131, FUJIFILM Wako) was added at 1.0 mM to both vehicle and MitoTEMPO groups to enhance porphyrin-derived autofluorescence, and MitoTEMPO (SML0737, Sigma-Aldrich) was added at 50 μM to the MitoTEMPO group; slices were incubated for 3 hours.

In vivo and *ex vivo* assessment of autofluorescence

In vivo autofluorescence was evaluated using an IVIS imaging system (PerkinElmer) under isoflurane anesthesia. Mice were epilated with Epilat cream (Kracie) before imaging. Standard *in vivo* imaging parameters were as follows: 710-nm excitation, 810- to 875-nm emission, 15-second exposure time, medium binning, and F/Stop 2. *Ex vivo* samples were analyzed similarly with a 5-second exposure time. For kidney slice imaging, the culture medium was replaced with phosphate-buffered saline, and 6 slices were stacked and imaged under the same conditions as *ex vivo* samples. Radiant efficiency (fluorescence emission relative to excitation intensity) was quantified. For *in vivo* and *ex vivo* mouse experiments, values were normalized to the mean of sham/control mice; for slice culture experiments, values were normalized to the mean of vehicle-treated slices.

Fluorescence analysis of porphyrin-related compounds

Porphyrin-related compounds were analyzed using the IVIS system with the following settings: 810- to 875-nm emission filter, 5-second exposure time, medium binning, and F/Stop 2. Excitation wavelengths ranged from 430 to 745 nm. The compounds tested were δ-ALA (FUJIFILM Wako), porphobilinogen, uroporphyrin I dihydrochloride, coproporphyrin I dihydrochloride (Sigma-Aldrich), coproporphyrin III dihydrochloride (Strem Chemicals), protoporphyrin IX disodium salt, biliverdin hydrochloride (Sigma-Aldrich), and bilirubin (FUJIFILM Wako). All compounds were prepared at 1.0 mM, with δ-ALA and porphobilinogen in distilled water and the others in ethanol. Measurements were performed in 96-well plates, and values were normalized to the mean value of water excited at 535 nm.

Porphyrin analysis by HPLC

Porphyrin metabolites were analyzed using high-performance liquid chromatography (HPLC), as previously described.[19] Briefly, tissue samples were homogenized in 200 μl of 0.1 M NaOH. Porphyrins were extracted by adding an N,N-dimethylformamide:isopropanol mixture (100:1, v/v) in a 1:3 ratio (v/v). The samples were stored overnight at room temperature in the dark. Porphyrin separation was achieved using an HPLC system equipped with a C18 reversed-phase column (5-μm particle size, 4.6 × 250 mm, Shiseido). The mobile phase consisted of Solvent A (1.0 M ammonium acetate with 12.5% acetonitrile, pH 5.2) and

Figure 2 | (continued) H2AX (γH2AX)–positive nuclei counts (n = 25). (**g**) Autofluorescence (pseudored) in frozen kidney sections counterstained with phalloidin (green), imaged on an Axio Observer microscope with a CSU-W1 confocal scanner (bar = 100 μm). Representative of 3 experiments. D, day; NS, not significant. To optimize viewing of this image, please see the online version of this article at www.kidney-international.org.

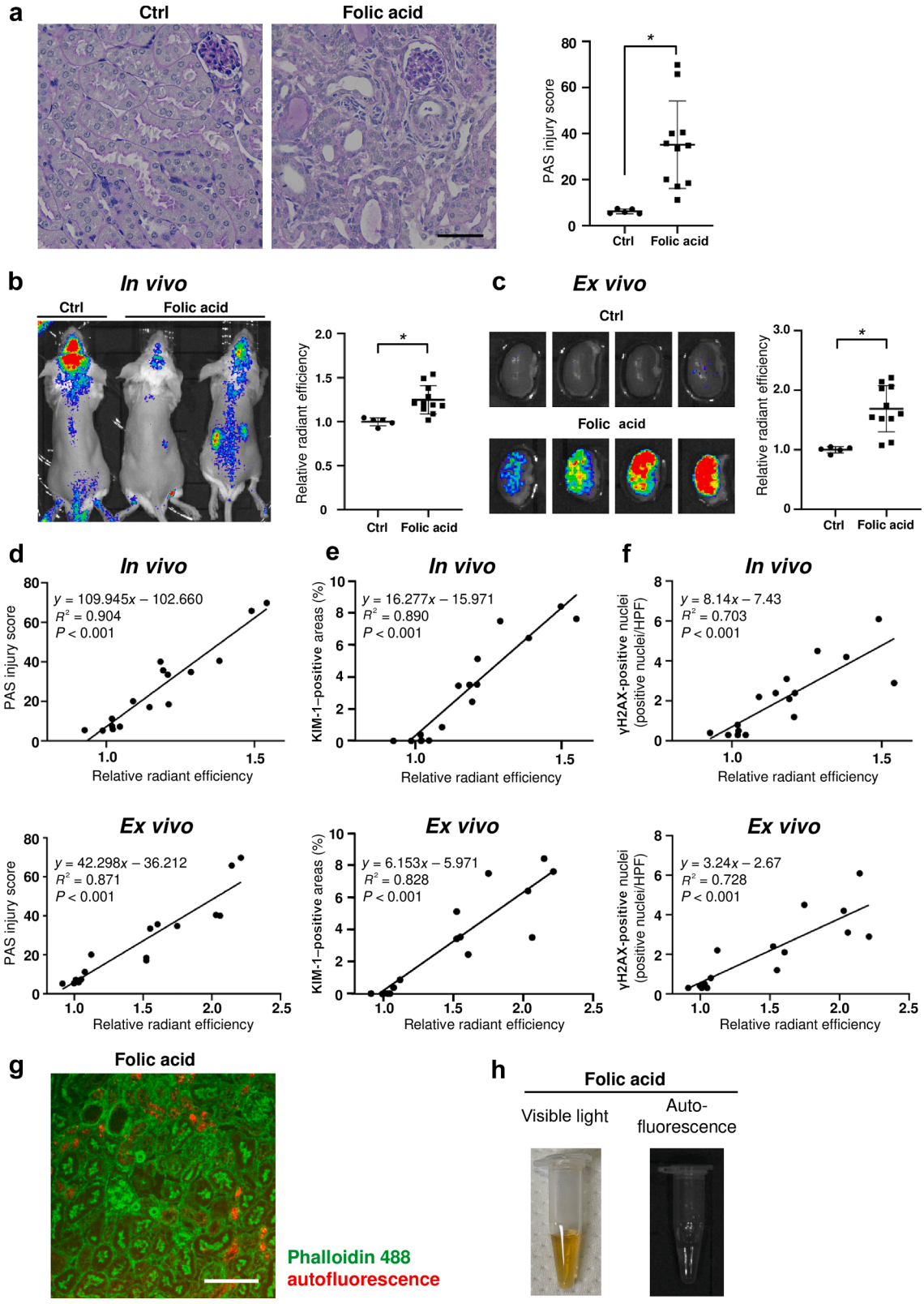


Figure 3 | Near-infrared autofluorescence correlates with tubular epithelial cell (TEC) injury in folic acid nephropathy. (**a**) TEC injury quantified by periodic acid–Schiff (PAS) staining on day 14 after injection. Representative images and quantification shown (control n = 5, folic acid n = 11; *$P < 0.05$, unpaired *t* test; bar = 100 μm). The folic acid model was originally performed with n = 12, but 1 sample was lost during histologic processing. (**b**) *In vivo* autofluorescence images (excitation: 710 nm, emission: 810–875 nm) and quantification (control n = 5, folic acid n = 11; *$P < 0.05$, unpaired *t* test). (**c**) *Ex vivo* autofluorescence images and quantification (control n = 5, folic acid (continued)

Solvent B (50 mM ammonium acetate with 80% acetonitrile, pH 5.2). Elution started with 100% Solvent A for 5 minutes, followed by a linear gradient to 100% Solvent B, and ended with 100% Solvent B for 10 minutes. The flow rate was 1.0 ml/min. Quantification was performed using external calibration curves.

Histologic analyses

Paraffin-embedded kidney sections were stained with periodic acid–Schiff (PAS) and Masson trichrome following standard protocols to assess tubular injury and fibrosis, respectively. Immunohistochemistry for KIM-1 (AF1817, R&D Systems) and phosphorylated histone H2AX (γH2AX) (05-636, Merck) was performed, as previously described,[20,21] to evaluate tubular injury and oxidative stress, respectively.

PAS- and Masson trichrome–stained sections were imaged on a Nikon Ni microscope. Tubular injury was quantified in PAS-stained kidney cortex sections (×200 magnification) using a 120-point (12 × 10) grid overlay. The number of grid points overlying atrophic or necrotic tubular cells was counted and expressed as PAS injury scores. Ten randomly selected fields were analyzed for each kidney. Tubulointerstitial fibrosis was quantified as the blue-stained area in Masson trichrome sections. Fifteen random cortical fields per kidney were analyzed. KIM-1–positive areas were quantified to evaluate the extent of TEC injury. γH2AX-positive nuclei were counted in 10 random cortical fields per kidney at ×200 magnification on an ECLIPSE E600 microscope (Nikon) for oxidative stress assessment. For lipofuscin evaluation, deparaffinized formalin-fixed, paraffin-embedded tissue sections were directly examined.

Immunofluorescence imaging

Immunofluorescence-stained sections were imaged on a FLUOVIEW FV3000 confocal microscope (Evident Scientific). The primary antibodies used were anti-megalin (31012, BiCell Scientific), anti-uromodulin (AF5175, R&D Systems), anti–KIM-1 (AF1817, R&D Systems), anti-coproporphyrinogen oxidase (CPOX) (12211-1-AP, Proteintech), anti–calbindin-D28k (214 004, SYSY antibodies), and anti–aquaporin 2 (20102, Bicell Scientific).

Autofluorescence microscopy

For autofluorescence microscopy, fresh frozen kidney sections were stained with phalloidin 488 (Thermo Fisher Scientific) to provide structural context. In the initial experiments, samples were imaged on an Axio Observer microscope (Carl Zeiss) equipped with a CSU-W1 confocal scanner (Yokogawa Electric). Owing to instrument unavailability during the revision, high-power field autofluorescence imaging in subsequent experiments was performed on a TCS SP8 X FALCON system (Leica Microsystems), with slightly different excitation conditions.

Serum biochemistry

Serum creatinine was measured with the DICT-500 kit (BioAssay Systems). Blood urea nitrogen was measured with the L-type Wako UN·V kit (463-55401, FUJIFILM Wako).

Quantitative reverse transcription–polymerase chain reaction (real-time polymerase chain reaction)

mRNA expression was quantified by real-time SYBR Green polymerase chain reaction on a QuantStudio 7 system (Applied Biosystems). Total RNA was extracted from kidney tissue with TRIzol reagent (Invitrogen), according to the manufacturer's instructions. Primer sequences are listed in Supplementary Table S1.

Western blot analysis

Tissue proteins were extracted using Cell Lysis Buffer (Cell Signaling Technology) supplemented with a protease inhibitor cocktail (Roche) and 1.0 mM phenylmethylsulfonyl fluoride. Western blot analysis was performed as previously described,[22,23] using anti-CPOX (12211-1-AP, Proteintech) and anti–glyceraldehyde-3-phosphate dehydrogenase (GTX100118, GeneTex) as primary antibodies.

Statistical analyses

Data are presented as mean ± SD. Statistical significance was evaluated using the unpaired *t* test, Dunnett test, Tukey-Kramer method, or Jonckheere-Terpstra trend test, as appropriate. For human kidney samples, all available specimens were analyzed as an exploratory proof-of-concept study without a predetermined sample size. Statistical significance was set at $P < 0.05$. Analyses were performed using JMP Pro 17.1.0 (SAS Institute) or EZR for Windows.

RESULTS

NIR autofluorescence detects kidney injury in the UUO model

We noninvasively evaluated kidney NIR autofluorescence using an IVIS imaging system in wild-type BALB/c mice on day 7 after UUO (Figure 1a). Renal autofluorescence was assessed using excitation filters ranging from 430 to 745 nm with an 810- to 875-nm emission filter (Figure 1a). Excitation at 710 nm yielded the strongest signal from injured kidneys, with weaker signals observed at 675 and 640 nm. No signal

Figure 3 | (continued) n = 11; *$P < 0.05$, unpaired *t* test). (**d–f**) Correlations between autofluorescence and (**d**) PAS injury scores, (**e**) kidney injury molecule (KIM)-1–positive areas, and (**f**) Phosphorylated histone H2AX (γH2AX)–positive nuclei counts (n = 16 total). (**g**) Autofluorescence (pseudored) in injured TECs with phalloidin counterstain (green), imaged on an Axio Observer microscope with a CSU-W1 confocal scanner (bar = 100 μm). (**h**) Folic acid solution (0.3 mol/l $NaHCO_3$) under visible light and IVIS imaging conditions (PerkinElmer) showing no detectable autofluorescence. Ctrl, control. To optimize viewing of this image, please see the online version of this article at www.kidney-international.org.

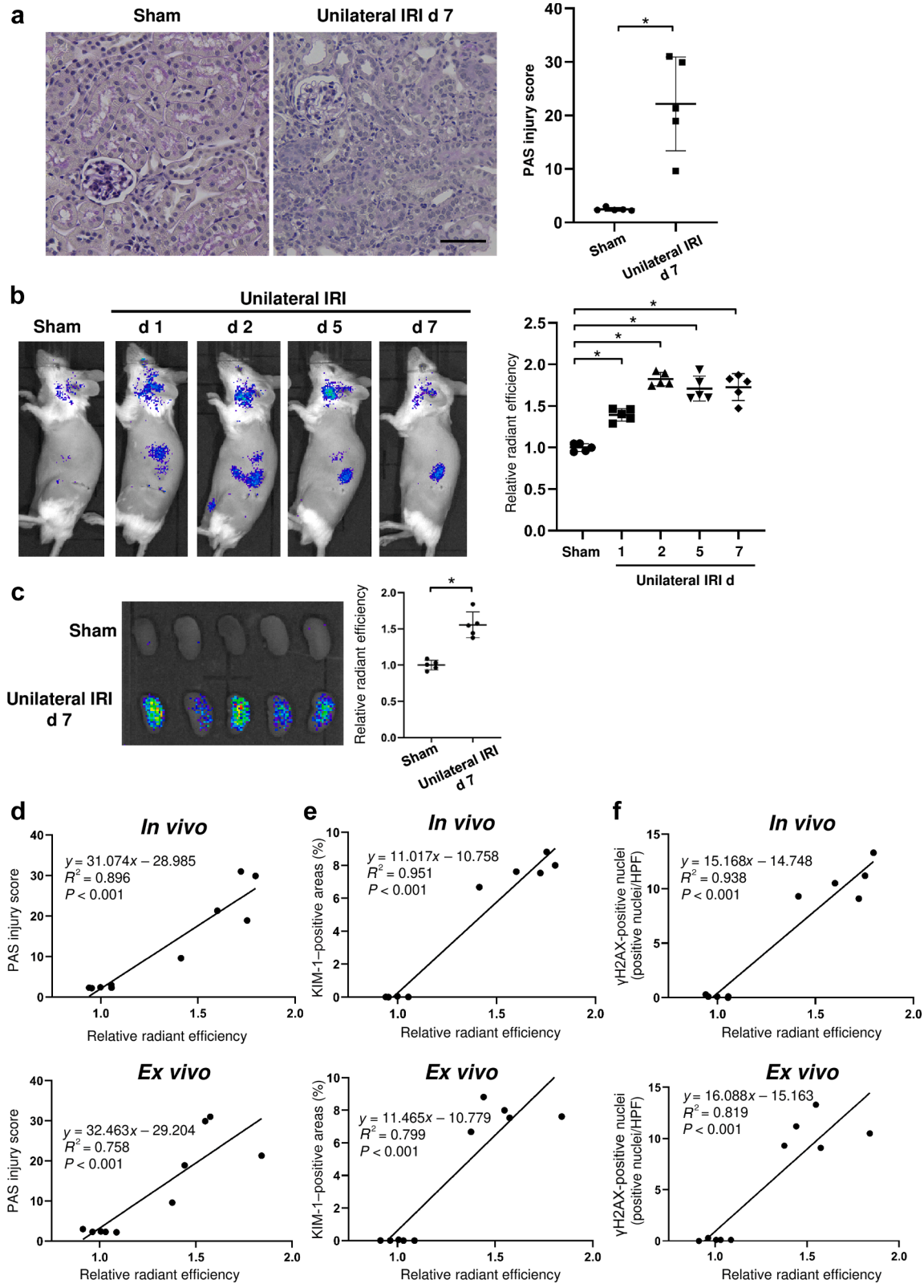


Figure 4 | Near-infrared autofluorescence correlates with tubular epithelial cell (TEC) injury in the unilateral ischemia-reperfusion injury (IRI) model. (**a**) TEC injury quantified by periodic acid–Schiff (PAS) staining on day (d) 7 after unilateral IRI. Representative images and quantification shown (n = 5 per group; *$P < 0.05$, unpaired *t* test; bar = 100 μm). (**b**) Longitudinal *in vivo* autofluorescence images (excitation: 710 nm, emission: 810–875 nm) and quantification (n = 5 per timepoint; *$P < 0.05$, Dunnett test). (**c**) *Ex vivo* autofluorescence images and quantification on d 7 (n = 5 per group; *$P < 0.05$, unpaired *t* test). (**d–f**) Correlations between autofluorescence and (**d**) PAS injury scores, (**e**) kidney injury molecule (KIM)-1–positive areas, and (**f**) Phosphorylated histone H2AX (γH2AX)–positive nuclei counts (n = 10 total). To optimize viewing of this image, please see the online version of this article at www.kidney-international.org.

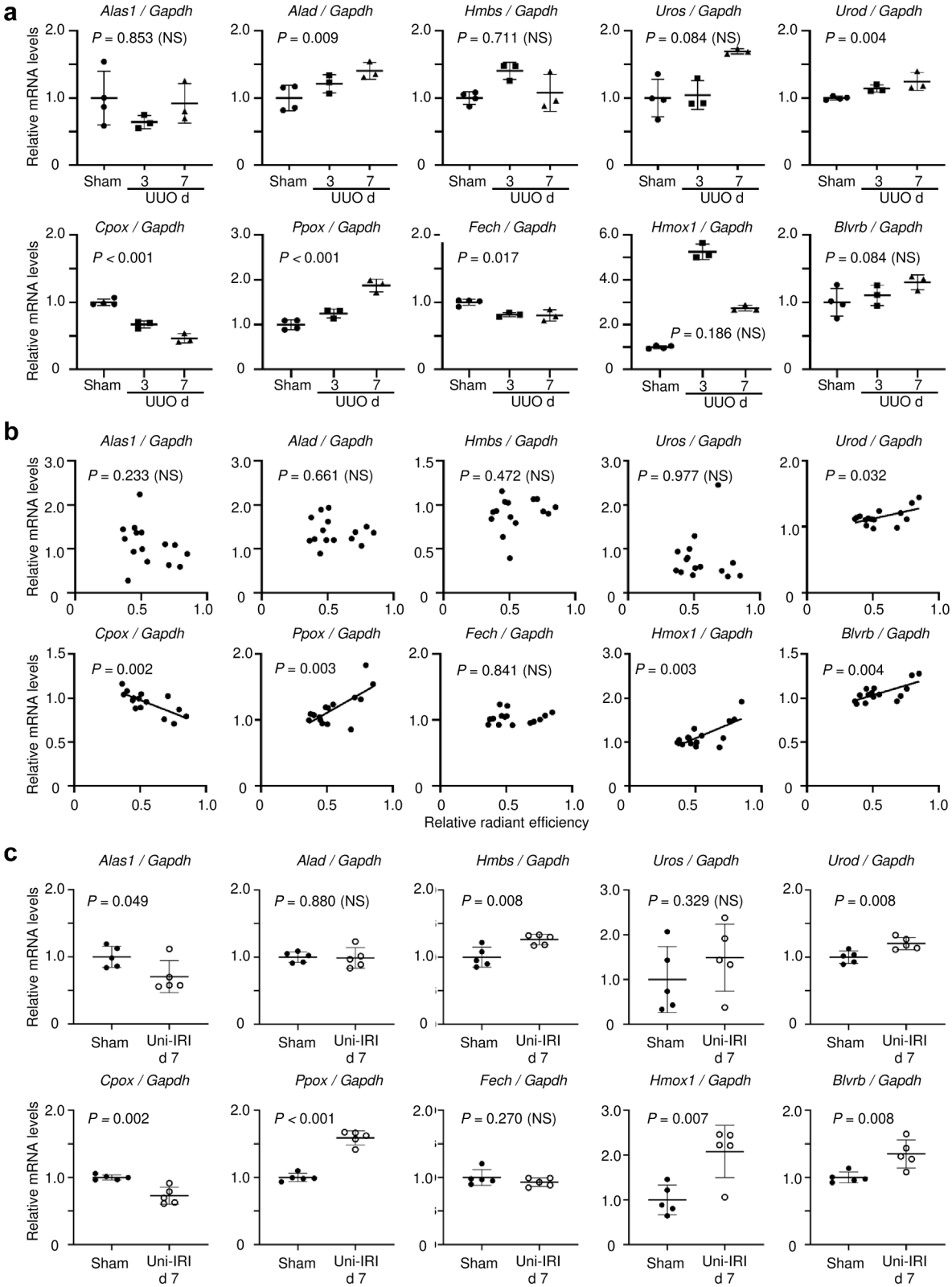


Figure 5 | *Cpox* downregulation associates with near-infrared autofluorescence in injured kidneys. (**a**) Renal expression of porphyrin biosynthesis enzymes by real-time polymerase chain reaction (PCR) in the unilateral ureteral obstruction (UUO) model (sham, day [d] 3, d 7; n = 3–4 per time point; Jonckheere-Terpstra trend test). The animals used for this analysis were from a separate cohort from those presented in Figure 2, accounting for the different n numbers. (**b**) Correlation between enzyme expression and autofluorescence intensity (excitation: 710 nm, emission: 810–875 nm) in folic acid nephropathy (control n = 3, folic acid n = 12; Pearson correlation). As described in the Figure 3 legend, the folic acid experiment was performed with control n = 5 and folic acid n = 12, but 2 control samples were lost during processing, resulting in control n = 3, folic acid n = 12 for this analysis. (**c**) Renal expression of porphyrin biosynthesis enzymes by real-time PCR in the unilateral ischemia-reperfusion injury model (Uni-IRI) (sham vs. d 7; n = 5 per group; unpaired *t* test). NS, not significant.

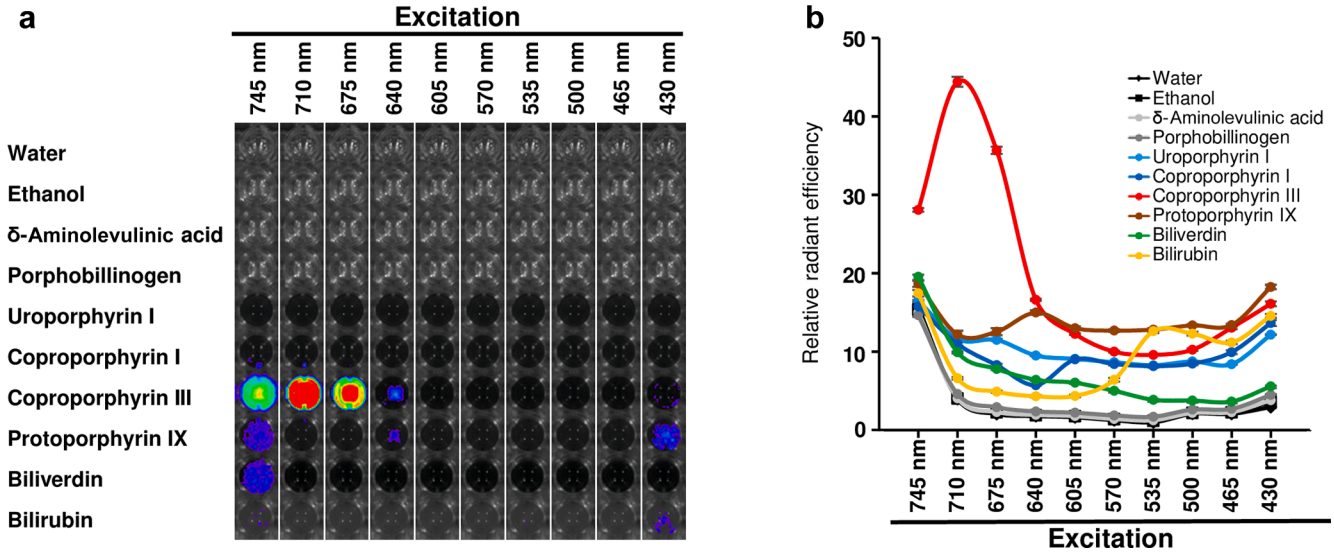


Figure 6 | Coproporphyrin III exhibits autofluorescence matching injured kidneys. (**a**) Autofluorescence of porphyrin-related metabolites and solvents under the same excitation and emission settings used for kidney imaging. Dynamic range of radiant efficiency: 1.75E+7 to 4.00E+7 p/s/cm^2/sr per μW/cm^2. (**b**) Quantified autofluorescence normalized to water autofluorescence at 535-nm excitation.

was detectable at excitation wavelengths below 605 nm. At 745-nm excitation, bleed-through from the excitation light saturated the detector and masked any kidney-derived signal (Figure 1a), and adjusting the dynamic range did not resolve this (Supplementary Figure S1). *Ex vivo* imaging of kidneys excised on day 7 after UUO confirmed that the signal originated from the injured kidneys (Figure 1b). To rule out contributions from other organs, we imaged various organs from UUO mice under the same conditions (excitation: 710 nm, emission: 810–875 nm; Figure 1c). Only the liver showed slight fluorescence, whereas other organs, except the UUO kidney, were nonfluorescent, confirming that the signal in Figure 1a was kidney specific.

Autofluorescence intensity correlates with kidney injury severity across multiple models

We next asked whether kidney autofluorescence tracks the severity of tubular injury, testing this across 3 mechanistically distinct models.

In the UUO model, PAS-stained sections showed progressive worsening of TEC injury (Figure 2a), and Masson trichrome staining revealed a parallel increase in tubulointerstitial fibrosis (Supplementary Figure S2A and B). Renal autofluorescence, visualized *in vivo* and *ex vivo*, likewise increased over time (Figure 2b and c). Autofluorescence correlated positively with PAS injury scores (Figure 2d), KIM-1–positive areas (Figure 2e), γH2AX-positive nuclei (Figure 2f), and Masson trichrome–positive areas (Supplementary Figure S2C). Because the contralateral kidney remained intact and maintained kidney function, autofluorescence did not correlate with serum urea nitrogen in this model (Supplementary Figure S2D). To determine the cellular origin of increased autofluorescence, we imaged fresh frozen sections at 685-nm excitation and 720- to 870-nm emission, the closest available wavelengths to our *in vivo* imaging parameters. Enhanced autofluorescence (pseudored) was seen in TECs on UUO day 7 (Figure 2g). Additional confocal imaging with comparable excitation conditions (excitation: 670 nm, emission: 715–800 nm) showed that the autofluorescence originated from the tubular cell bodies themselves rather than from intraluminal casts or debris in phalloidin-counterstained frozen sections (Supplementary Figure S2E). The autofluorescence was minimal in proximal tubular cells with strong megalin expression, whereas it was evident in cells with weak megalin staining or KIM-1 positivity, indicating that the signal arises from injured rather than intact proximal tubules. No autofluorescence was observed in uromodulin-positive distal tubules.

We also asked whether the signal is detectable in C57BL/6J mice. On day 7, these mice showed TEC injury by PAS staining (Supplementary Figure S3A). *In vivo* autofluorescence was elevated in UUO kidneys from day 1 onward, and *ex vivo* imaging on day 7 confirmed a signal increase (Supplementary Figure S3B and C). Autofluorescence in sham and UUO day 7 kidneys correlated with PAS injury scores, KIM-1–positive areas, and γH2AX-positive nuclei (Supplementary Figure S3D–F). The signal was thus detectable despite the dark coat color of this strain.

The folic acid nephropathy model, which shows greater interindividual variability than UUO, allowed us to test whether the relationship holds across a range of injury severities in wild-type BALB/c mice. PAS and Masson trichrome staining confirmed tubulointerstitial injury on day 14 with substantial variability (Figure 3a and Supplementary Figure S4A and B).[24] Mean autofluorescence in folic acid–injected mice was higher than in controls (Figure 3b and

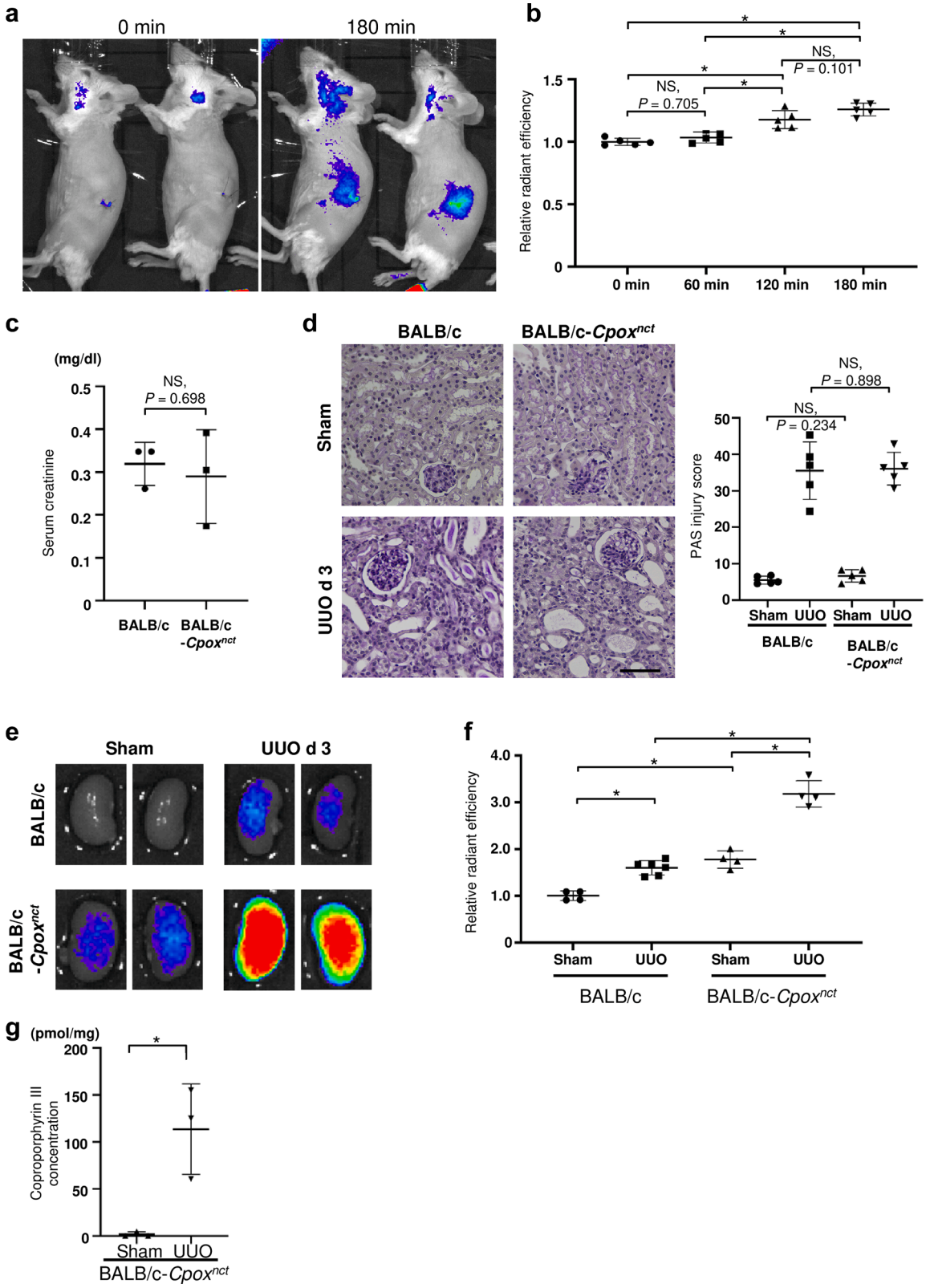


Figure 7 | Reduced coproporphyrinogen oxidase activity enhances autofluorescence. (**a**) *In vivo* autofluorescence images (excitation: 710 nm, emission: 810–875 nm) of wild-type unilateral ureteral obstruction (UUO) mice on day (d) 3, before and 180 minutes after i.p. δ-aminolevulinic acid (δ-ALA) injection (300 mg/kg). (**b**) Time course of autofluorescence after δ-ALA injection, normalized to baseline (n = 5 per group; **P* < 0.05, Tukey-Kramer test). (**c**) Serum creatinine in wild-type BALB/c and BALB/c-*Cpox*^{nct} mice at baseline (n = 3 per group; unpaired *t* test). (**d**) Tubular epithelial cell injury quantified by periodic acid–Schiff (PAS) staining in sham and UUO d 3 kidneys from both genotypes (n = 5 per group; unpaired *t* test; bar = 100 μm). (**e**) *Ex vivo* autofluorescence images of kidneys (continued)

c), and the signal correlated with PAS injury scores, KIM-1–positive areas, γH2AX-positive nuclei (Figure 3d–f), Masson trichrome–positive areas, serum creatinine levels, and serum urea nitrogen (Supplementary Figure S4C–E). As in UUO kidneys, the autofluorescence localized to TECs (Figure 3g and Supplementary Figure S4F). Folic acid itself gave no detectable fluorescence under our imaging conditions (Figure 3h).

The unilateral IRI model extended this validation to acute injury. PAS staining on day 7 confirmed TEC damage (Figure 4a). Longitudinal *in vivo* imaging showed that autofluorescence increased from day 1 and peaked on day 2 (Figure 4b), and *ex vivo* imaging on day 7 confirmed persistent elevation (Figure 4c). The signal again correlated with PAS injury scores, KIM-1–positive areas, γH2AX-positive nuclei (Figure 4d–f), and Masson trichrome–positive areas, and localized to TECs (Supplementary Figure S5A–C). Because the contralateral kidney maintained renal function, serum urea nitrogen did not correlate with autofluorescence intensity in this model (Supplementary Figure S5D). Together, these results show that NIR autofluorescence quantitatively reflects kidney injury across different injury mechanisms and mouse strains.

Reduced *Cpox* expression associates with NIR autofluorescence in injured kidneys

Porphyrins are among the endogenous fluorophores with emission in the long-wavelength region.[18] We analyzed renal mRNA expression levels of porphyrin biosynthesis enzymes in all 3 injury models (Figure 5 and Supplementary Figure S6). Although several enzymes were upregulated, *Cpox* mRNA, encoding coproporphyrinogen (CPG) oxidase, a mitochondrial enzyme that catalyzes the oxidation of CPG III to protoporphyrinogen IX, was consistently reduced with TEC injury progression in UUO and unilateral IRI models (Figure 5a and c). In folic acid nephropathy, *Cpox* mRNA was inversely correlated with autofluorescence intensity (Figure 5b), although the difference between control and folic acid groups did not reach statistical significance when compared as 2 groups (Supplementary Figure S7A), likely owing to the large interindividual variability of this model. At the protein level, however, Western blot analysis showed reduced CPOX expression in injured kidneys across all 3 models, including folic acid nephropathy, where both a group difference and a negative correlation with autofluorescence were observed (Supplementary Figure S7B). To identify which tubular segments express CPOX, we performed immunofluorescence costaining with segment-specific markers. CPOX was absent from calbindin-D28k–positive distal convoluted tubules, uromodulin-positive thick ascending limb cells, and aquaporin 2–positive collecting duct cells (Supplementary Figure S8A). Costaining with megalin confirmed proximal tubular localization of CPOX and showed that CPOX staining was markedly reduced in injured kidneys across all 3 models (Supplementary Figure S8B), consistent with the Western blot data (Supplementary Figure S7B). The cellular site of CPOX downregulation thus matches the site of enhanced NIR autofluorescence identified by costaining experiments (Supplementary Figure S2E). These findings suggested accumulation of CPG III and its spontaneously oxidized product, coproporphyrin III, in injured kidneys.

We evaluated fluorescence of authentic porphyrin-related metabolites (Figure 6a). Only coproporphyrin III exhibited autofluorescence similar to that observed in injured kidneys. Quantitative analysis showed that coproporphyrin III autofluorescence peaked at 710-nm excitation (Figure 6b), matching our *in vivo* imaging conditions. Coproporphyrin III accumulation resulting from reduced *Cpox* expression is thus the likely source of enhanced autofluorescence in injured kidneys.

Because lipofuscin also exhibits autofluorescence, we evaluated its presence in kidney tissue. Although 12-month-old rats (positive control) showed lipofuscin deposition in TECs, no lipofuscin accumulation was detected in TECs from any of our kidney injury models (Supplementary Figure S9).

Reduced CPG oxidase activity enhances NIR autofluorescence in kidneys

To test the role of coproporphyrin III in kidney autofluorescence, we i.p. injected δ-ALA, a porphyrin precursor, into UUO mice on day 3. Although δ-ALA itself was nonfluorescent (Figure 6a), its administration enhanced autofluorescence in UUO kidneys (Figure 7a and b).

We next examined BALB/c-*Cpox*^{nct} mice, which harbor a missense mutation in *Cpox* that reduces CPG oxidase activity to <15% of the wild-type level.[25] This mutation did not affect baseline kidney function (Figure 7c) or alter UUO-induced kidney injury, as assessed by PAS and Masson trichrome staining (Figure 7d and Supplementary Figure S10). Even so, sham-operated kidneys of BALB/c-*Cpox*^{nct} mice showed higher autofluorescence than those of wild-type BALB/c mice, and this signal was further increased in UUO day 3 kidneys (Figure 7e and f). Renal coproporphyrin III concentrations were elevated in UUO day 3 kidneys of BALB/c-*Cpox*^{nct} mice compared with sham-operated controls (Figure 7g). Thus, reduced CPG oxidase activity leads to coproporphyrin III accumulation and enhanced NIR autofluorescence in injured kidneys.

Figure 7 | (continued) from wild-type and BALB/c-*Cpox*^{nct} mice under sham and UUO conditions. (**f**) Quantified autofluorescence from (**e**), normalized to wild-type sham controls (n = 4–6 per group; *$P < 0.05$, Tukey-Kramer test). The n numbers in (**d**) and (**e,f** differ because autofluorescence imaging was performed first without tissue collection; histologic analysis was subsequently performed using a separate cohort. (**g**) Renal coproporphyrin III concentrations in BALB/c-*Cpox*^{nct} mice under sham and UUO d 3 conditions (n = 3 per group; *$P < 0.05$, unpaired *t* test). NS, not significant. To optimize viewing of this image, please see the online version of this article at www.kidney-international.org.

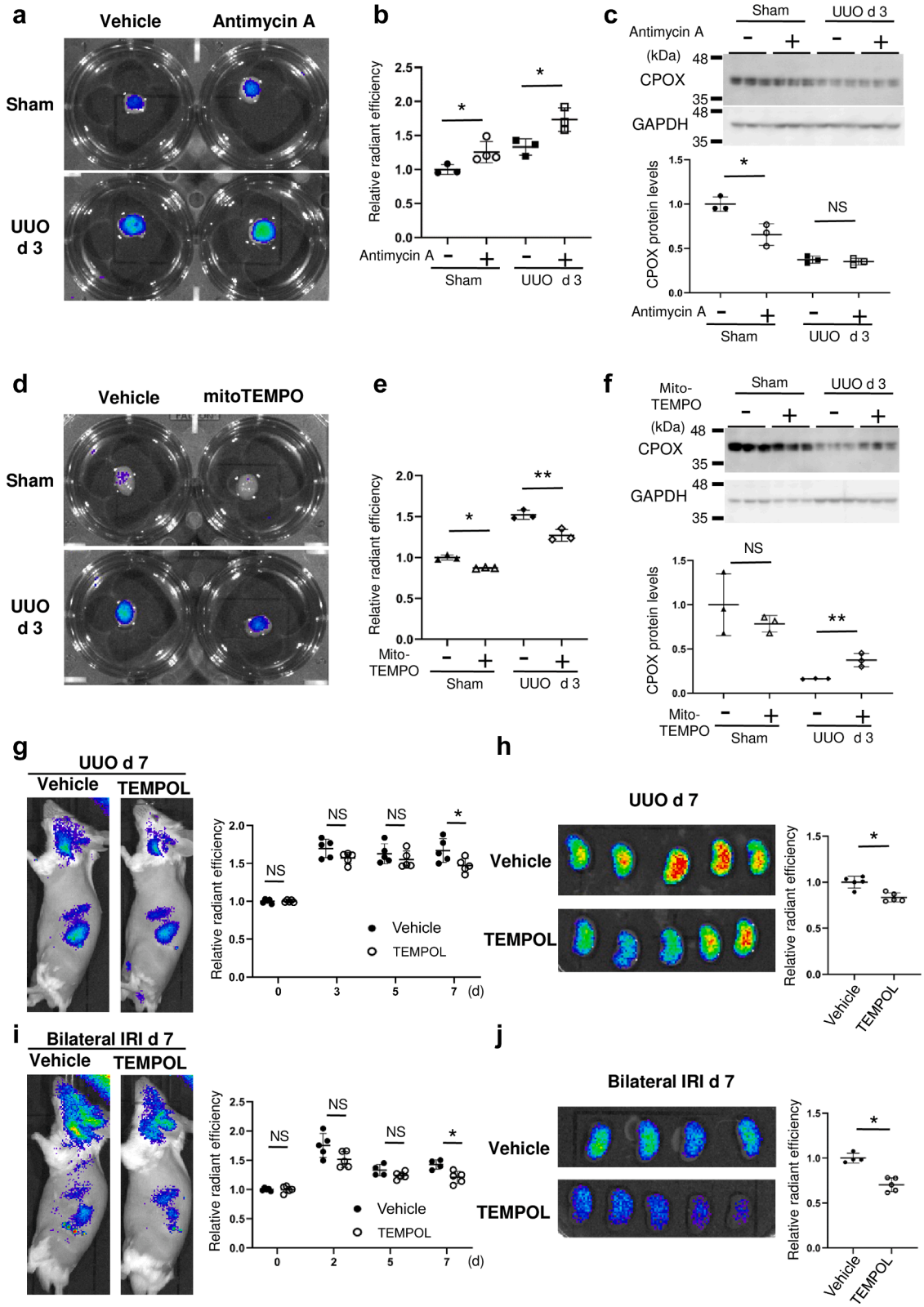


Figure 8 | Mitochondrial dysfunction and oxidative stress drive near-infrared autofluorescence in injured kidneys. (**a**) Representative autofluorescence images of kidney slices from sham and unilateral ureteral obstruction (UUO) day (d) 3 mice, treated with vehicle or antimycin A. (**b**) Quantification of (**a**) (n = 3–4 per group; *$P < 0.05$, unpaired *t* test). (**c**) Western blot analysis of coproporphyrinogen oxidase (CPOX) and glyceraldehyde-3-phosphate dehydrogenase (GAPDH) in kidney slices, with densitometric quantification (n = 3 per group; *$P <$ 0.05, unpaired *t* test). The slices used for Western blot in (**c**) were separate from those used for autofluorescence quantification (continued)

Mitochondrial dysfunction and oxidative stress drive NIR autofluorescence in injured kidneys

To further investigate the mechanism underlying enhanced autofluorescence, we used a kidney slice culture system from UUO day 3 mice. Inhibition of the mitochondrial electron transport chain with antimycin A enhanced autofluorescence in both sham and UUO day 3 slices (Figure 8a and b). In sham slices, antimycin A reduced CPOX protein expression. In UUO day 3 slices, however, CPOX was already lower than in sham slices at baseline, and antimycin A did not reduce it further (Figure 8c). Conversely, scavenging of mitochondrial reactive oxygen species with MitoTEMPO reduced autofluorescence in both sham and UUO day 3 slices (Figure 8d and e). MitoTEMPO did not affect CPOX protein in sham slices but partially rescued its expression in UUO day 3 slices (Figure 8f). These results suggest that mitochondrial oxidative stress suppresses CPOX expression and that, even at a given CPOX level, greater oxidative stress amplifies the autofluorescence signal. This is consistent with a mechanism in which reduced CPOX expression promotes accumulation of coproporphyrinogen III, which is then spontaneously oxidized to coproporphyrin III, the likely source of enhanced NIR autofluorescence.

We next asked whether reducing oxidative stress *in vivo* attenuates the autofluorescence signal. TEMPOL was administered in drinking water from day 5 to day 7 in both UUO and bilateral IRI models. We chose this narrow treatment window specifically to assess the effect of oxidative stress reduction on autofluorescence without allowing time for structural repair. In UUO mice, TEMPOL reduced *in vivo* autofluorescence on day 7 (Figure 8g), and *ex vivo* autofluorescence of TEMPOL-treated UUO kidneys was lower than that of vehicle-treated UUO kidneys on day 7 (Figure 8h). In bilateral IRI mice, TEMPOL similarly attenuated *in vivo* and *ex vivo* autofluorescence on day 7 (Figure 8i and j). PAS injury scores were comparable between vehicle- and TEMPOL-treated mice in both models (Supplementary Figure S11), indicating that autofluorescence captured the early molecular response to oxidative stress reduction even before histologic changes became apparent. These results establish that mitochondrial dysfunction and oxidative stress drive CPOX downregulation and coproporphyrin III–derived autofluorescence in injured kidneys.

NIR autofluorescence detects therapeutic responses

To test whether autofluorescence can track therapeutic efficacy noninvasively, we treated UUO mice with finerenone.[26] Finerenone reduced TEC injury and tubulointerstitial fibrosis on UUO day 7, as assessed by PAS and Masson trichrome staining (Figure 9a and b and Supplementary Figure S12). Finerenone reduced expression of kidney injury markers and fibrosis-related genes, although the reductions in mRNA levels were modest (Figure 9c). Finerenone-treated mice showed lower kidney autofluorescence than vehicle-treated controls on days 4, 6, and 7 after UUO by *in vivo* imaging (Figure 9d and e), and *ex vivo* analysis on day 7 confirmed the reduction (Figure 9f and g).

We further asked whether NIR autofluorescence can detect therapeutic responses in bilateral IRI, a model in which kidney function can be assessed by serum markers (Supplementary Figure S13). Finerenone reduced PAS injury scores on bilateral IRI day 7 (Supplementary Figure S13A). Longitudinal *in vivo* imaging showed lower autofluorescence in finerenone-treated mice from day 2 onward (Supplementary Figure S13B), although the difference was not apparent on day 5, likely because 1 mouse with high autofluorescence in the vehicle group died after the day 2 measurement. *Ex vivo* autofluorescence on day 7 was lower in finerenone-treated kidneys (Supplementary Figure S13C) and correlated positively with both serum creatinine and urea nitrogen (Supplementary Figure S13D and E). These results show that NIR autofluorescence tracks with therapeutic response across different injury models.

Human kidney autofluorescence correlates with injury markers

To investigate potential clinical applications, we analyzed nontumor regions of kidney samples from patients who underwent nephrectomy for malignant tumors. NIR autofluorescence varied among samples (Figure 10a). Lower estimated glomerular filtration rate was associated

Figure 8 | (continued) in (**b**), because the time and oxygen and/or temperature changes during autofluorescence measurement could potentially affect protein expression; this accounts for the different n numbers between (**b**) and (**c**). (**d**) Representative autofluorescence images of kidney slices from sham and UUO d 3 mice, treated with vehicle or MitoTEMPO. (**e**) Quantification of (**d**) (n = 3 per group; $^*P < 0.05$, unpaired *t* test). (**f**) Western blot analysis of CPOX and GAPDH in kidney slices, with densitometric quantification (n = 3 per group; $^*P < 0.05$, unpaired *t* test). The slices used for (**e**) and (**f**) were also prepared separately for the same reason, although the n numbers are the same. (**g**) UUO mice received vehicle or 4-hydroxy-2,2,6,6-tetramethylpiperidine-1-oxyl (TEMPOL) in drinking water from d 5 to d 7. Representative *in vivo* autofluorescence images on d 7, with quantification on d 0, 3, 5, and 7 (n = 5 per group; $^*P < 0.05$, unpaired *t* test). (**h**) *Ex vivo* autofluorescence images and quantification of vehicle-treated and TEMPOL-treated UUO d 7 kidneys (n = 5 per group; $^*P < 0.05$, unpaired *t* test). (**i**) Bilateral ischemia-reperfusion injury (IRI) mice received vehicle or TEMPOL in drinking water from d 5 to d 7. Representative *in vivo* autofluorescence images on d 7, with quantification on d 0, 2, 5, and 7 (vehicle n = 4–5, TEMPOL n = 5; $^*P < 0.05$, unpaired *t* test). One mouse in the vehicle group died after the d 2 measurement, resulting in n = 4 for d 5 and d 7. (**j**) *Ex vivo* autofluorescence images and quantification of vehicle- and TEMPOL-treated bilateral IRI d 7 kidneys (vehicle n = 4, TEMPOL n = 5; $^*P < 0.05$, unpaired *t* test). To optimize viewing of this image, please see the online version of this article at www.kidney-international.org.

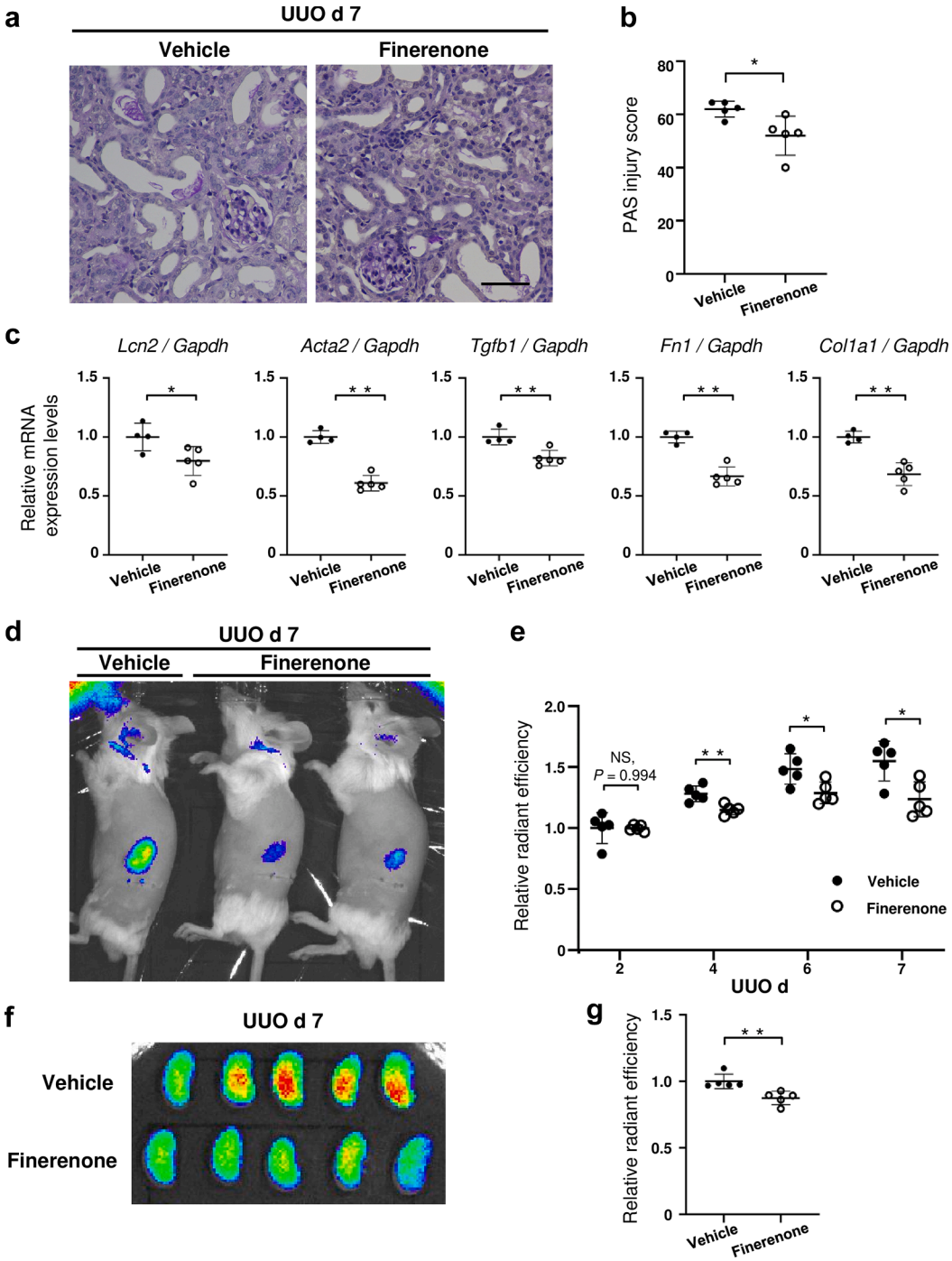


Figure 9 | Near-infrared autofluorescence reflects the therapeutic effects of finerenone in the unilateral ureteral obstruction (UUO) model. (**a**) Representative periodic acid–Schiff (PAS)–stained kidney sections of wild-type mice on UUO day (d) 7, treated with vehicle or finerenone (bar = 100 μm). (**b**) Quantified PAS injury scores (n = 5 per group; *$P < 0.05$, unpaired *t* test). (**c**) Expression of kidney injury and fibrosis genes by real-time polymerase chain reaction (n = 4–5 per group; *$P < 0.05$, **$P < 0.01$, unpaired *t* test). (**d**) Representative *in vivo* autofluorescence images (excitation: 710 nm, emission: 810–875 nm) of UUO d 7 mice with vehicle or finerenone treatment. (**e**) Quantified *in vivo* autofluorescence in vehicle- and finerenone-treated UUO mice, normalized to vehicle-treated d 2 (n = 5 per group; *$P < 0.05$, **$P < 0.01$, unpaired *t* test at each time point). (**f**) *Ex vivo* autofluorescence images of UUO d 7 kidneys from vehicle- and finerenone-treated mice. (**g**) Quantified *ex vivo* autofluorescence from (**f**), normalized to vehicle controls (n = 5 per group; **$P < 0.01$, unpaired *t* test). NS, not significant.

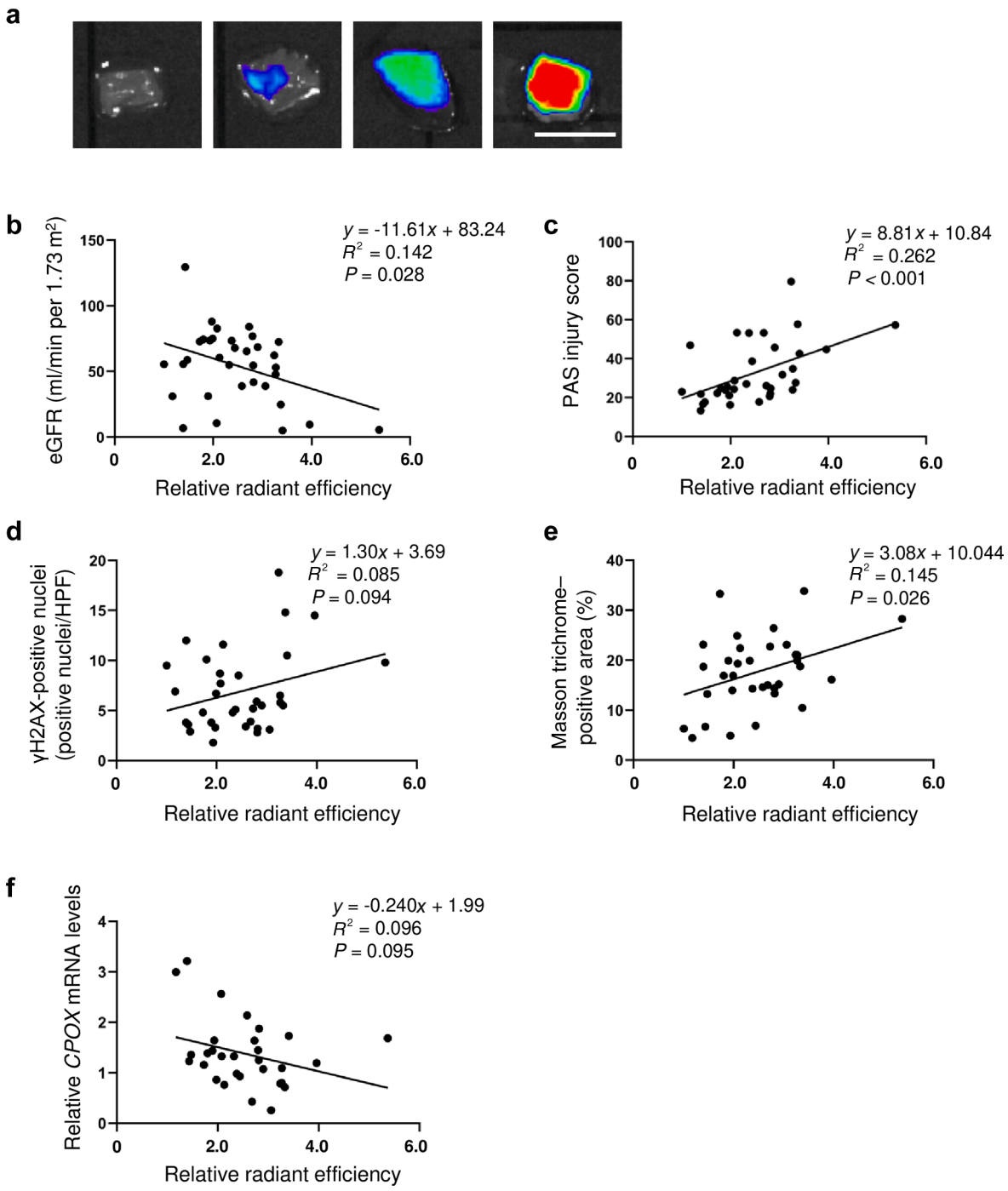


Figure 10 | Near-infrared autofluorescence in human kidney samples correlates with injury markers. (**a**) Representative autofluorescence images of resected human kidney samples showing varying intensity (bar = 1.0 cm). Dynamic range of radiant efficiency: 6.50E+6 to 1.50E+7 p/s/cm^2/sr per μW/cm^2. (**b–f**) Correlations between autofluorescence intensity and (**b**) estimated glomerular filtration rate (eGFR; n = 34, $P = 0.028$), (**c**) periodic acid–Schiff (PAS) injury scores (n = 34, $P < 0.001$), (**d**) Phosphorylated histone H2AX (γH2AX)–positive nuclei counts (n = 34, $P = 0.094$), (**e**) Masson trichrome–positive areas (n = 34, $P = 0.034$), and (**f**) *CPOX* mRNA expression (n = 34, $P = 0.095$).

with higher autofluorescence (Figure 10b), and autofluorescence increased with TEC injury on PAS staining (Figure 10c). A positive trend was observed between autofluorescence intensity and oxidative stress markers, although this did not reach statistical significance (Figure 10d). Masson trichrome–positive fibrotic areas correlated positively (Figure 10e), whereas *CPOX* mRNA expression showed a marginally significant negative association (Figure 10f). These results indicate that NIR autofluorescence correlates with established markers of kidney injury in humans, supporting its potential as a translatable biomarker.

DISCUSSION

Here, we show that NIR autofluorescence can quantify TEC injury without external agents. The signal originated specifically from injured proximal tubular cells and tracked histologic severity and oxidative stress across 3 models with different injury mechanisms. We identified coproporphyrin III accumulation, resulting from CPOX downregulation in injured TECs, as the likely molecular basis for the enhanced signal. Reduced autofluorescence in finerenone-treated kidneys showed that the method can track therapeutic responses, and the correlations seen in human kidney samples raise the possibility that similar mechanisms operate in humans.

CPG oxidase is an oxygen-dependent mitochondrial enzyme that catalyzes the oxidation of CPG III to protoporphyrinogen IX.[27–29] This oxygen dependence makes the enzyme sensitive to hypoxic conditions often associated with kidney injury.[30] Our mechanistic data go further: inhibiting the mitochondrial electron transport chain with antimycin A reduced CPOX protein and increased autofluorescence in kidney slice cultures, whereas scavenging mitochondrial reactive oxygen species with MitoTEMPO had the opposite effect. *In vivo* TEMPOL administration attenuated autofluorescence without improving histologic injury scores, showing that oxidative stress contributes to signal intensity independently of structural damage. These data support a model in which mitochondrial dysfunction generates reactive oxygen species that suppress CPOX, allowing coproporphyrinogen III to accumulate and oxidize spontaneously to the NIR-fluorescent coproporphyrin III. Unlike kidney biopsy or imaging approaches requiring exogenous probes, this method exploits endogenous signals, which simplifies preclinical workflows and may ease clinical translation.

NIR fluorescence imaging offers practical advantages for both preclinical and clinical work, including deep tissue penetration, minimal photodamage, and high sensitivity.[17,31–33] Indocyanine green is widely used for surgical guidance but requires injection and carries regulatory constraints.[34–38] Autofluorescence requires no such agents. NIR autofluorescence has also shown promise for identifying high-risk atherosclerotic plaques in humans,[39] suggesting that endogenous fluorophores can yield useful clinical signals well beyond the kidney.

Several limitations merit discussion. First, although we demonstrated CPOX downregulation and coproporphyrin III accumulation in BALB/c-*Cpox*^{nct} mice, direct quantification of coproporphyrin III in wild-type injured kidneys proved technically challenging because of the hydrophobic nature of the compound, with most samples falling below HPLC detection thresholds. The interpretation of coproporphyrin III as the likely primary fluorophore in wild-type animals therefore relies on indirect evidence, including spectroscopic matching and CPOX downregulation, supported by direct HPLC quantification in BALB/c-*Cpox*^{nct} mice. More sensitive analytical methods may be needed. Second, although NIR light penetrates tissues more effectively than visible light, depth remains a constraint. Our approach is well suited for mouse models and potentially for superficial or endoscopically accessible tissues in larger animals and humans, but transcutaneous imaging of deep organs presents challenges. Third, whether the quantitative relationship between autofluorescence intensity and injury severity holds across different underlying causes of kidney disease will need to be tested in larger patient series. Fourth, microalbuminuria was not assessed in the current study; this remains a limitation to be addressed in future work. Fifth, for human kidney samples, autofluorescence was measured from frozen tissue pieces that were cut to a similar but not precisely controlled size, and signal intensity was not normalized to tissue weight or volume. We cannot exclude the possibility that size variability contributed to the scatter in the correlation analyses; weight-based normalization should be incorporated in future studies.

Catheter-based optic probes could extend the approach to native kidneys in a minimally invasive manner, and intraoperative imaging may allow real-time assessment of organ viability during transplantation or nephron-sparing surgery. For now, the most immediate application is in preclinical research, where longitudinal monitoring of kidney injury and drug responses becomes possible without serial sacrifice, reducing the number of animals required.

DISCLOSURE

HF is an employee of Astellas Pharma Inc. All the other authors declared no competing interests.

DECLARATION OF GENERATIVE AI AND AI-ASSISTED TECHNOLOGIES IN THE WRITING PROCESS

During the preparation of this work, the authors used Claude (Anthropic) to improve the language and readability of the manuscript. After using this tool, the authors reviewed and edited the content as needed and take full responsibility for the content of the publication.

DATA STATEMENT

All processed numerical data supporting the figures and supplementary figures are included in this published article and its supplementary information files. Raw imaging files and individual-level human clinical data have not been deposited in a public repository because unrestricted public release was not included in the approved consent and ethics framework and could compromise participant confidentiality. These restrictions are imposed by the Ethics Committee of the University of Osaka Medical Hospital (approval number 14317-2). Deidentified data are made available from the corresponding author on reasonable request, subject to institutional approval and applicable data transfer agreements.

ACKNOWLEDGMENTS

The authors thank Ms. Naoko Horimoto for her technical assistance. The authors are also grateful to the Center of Medical Research and

Education, Graduate School of Medicine, the University of Osaka, for technical support. The authors also thank the Live Imaging Center at Innovative Support Alliance for Life Science, Kyoto University, for support and collaboration.

FUNDING STATEMENT

This research was supported by a grant from Astellas Pharma, Inc. (Ibaraki, Japan), Konica Minolta Science and Technology Foundation, and JST-Mirai Program grant number JPMJMI23G1.

AUTHOR CONTRIBUTIONS

AM, IM, and HF conceptualized the study. AM, IM, HF, YKu, and S-IO performed investigations and methods. AM, IM, YKu, and S-IO performed formal analysis. AM, IM, and YKu performed data curation and visualization. IM acquired funding. AM and IM performed project administration. IM and KI performed validation. KI and YI supervised the study. AM and IM performed writing (original draft). IM, HF, YKu, NT, HO, AI, MS, TH, TK, KH, YKa, AK, S-IO, NN, KI, and YI performed writing (review and editing). AM, IM, YKu, NT, HO, AI, MS, TH, TK, KH, YKa, AK, NN, and KI provided resources.

Supplementary material is available online at www.kidney-international.org.

REFERENCES

1. Liu BC, Tang TT, Lv LL, et al. Renal tubule injury: a driving force toward chronic kidney disease. *Kidney Int*. 2018;93:568–579.
2. Nath KA. Tubulointerstitial changes as a major determinant in the progression of renal damage. *Am J Kidney Dis*. 1992;20:1–17.
3. Mackensen-Haen S, Bader R, Grund KE, et al. Correlations between renal cortical interstitial fibrosis, atrophy of the proximal tubules and impairment of the glomerular filtration rate. *Clin Nephrol*. 1981;15:167–171.
4. Risdon RA, Sloper JC, De Wardener HE. Relationship between renal function and histological changes found in renal-biopsy specimens from patients with persistent glomerular nephritis. *Lancet*. 1968;2:363–366.
5. Bonsib SM. Focal-segmental glomerulosclerosis: the relationship between tubular atrophy and segmental sclerosis. *Am J Clin Pathol*. 1999;111:343–348.
6. Coppo R, D'Arrigo G, Tripepi G, et al. Is there long-term value of pathology scoring in immunoglobulin A nephropathy? a validation study of the Oxford Classification for IgA Nephropathy (VALIGA) update. *Nephrol Dial Transplant*. 2020;35:1002–1009.
7. Taft JL, Nolan CJ, Yeung SP, et al. Clinical and histological correlations of decline in renal function in diabetic patients with proteinuria. *Diabetes*. 1994;43:1046–1051.
8. Dong J, Li Y, Yue S, et al. The profiles of biopsy-proven renal tubulointerstitial lesions in patients with glomerular disease. *Ann Transl Med*. 2020;8:1066.
9. Yang L, Besschetnova TY, Brooks CR, et al. Epithelial cell cycle arrest in G2/M mediates kidney fibrosis after injury. *Nat Med*. 2010;16:535–543.
10. Liu Y. Renal fibrosis: new insights into the pathogenesis and therapeutics. *Kidney Int*. 2006;69:213–217.
11. Lovisa S, LeBleu VS, Tampe B, et al. Epithelial-to-mesenchymal transition induces cell cycle arrest and parenchymal damage in renal fibrosis. *Nat Med*. 2015;21:998–1009.
12. Zhang Y, Yang Y, Yang F, et al. HDAC9-mediated epithelial cell cycle arrest in G2/M contributes to kidney fibrosis in male mice. *Nat Commun*. 2023;14:1–17.
13. Baues M, Klinkhammer BM, Ehling J, et al. A collagen-binding protein enables molecular imaging of kidney fibrosis *in vivo*. *Kidney Int*. 2020;97:609–614.
14. Park SY, Kim MW, Kang JH, et al. Novel NF-κB reporter mouse for the non-invasive monitoring of inflammatory diseases. *Sci Rep*. 2023;13:1–12.
15. Weissleder R. A clearer vision for *in vivo* imaging. *Nat Biotechnol*. 2001;19:316–317.
16. Doyle TC, Burns SM, Contag CH. Technoreview: *in vivo* bioluminescence imaging for integrated studies of infection. *Cell Microbiol*. 2004;6:303–317.
17. Shcherbakova DM, Verkhusha VV. Near-infrared fluorescent proteins for multicolor *in vivo* imaging. *Nat Methods*. 2013;10:751–754.
18. Christensen J, Nørgaard L, Bro R, et al. Multivariate autofluorescence of intact food systems. *Chem Rev*. 2006;106:1979–1994.
19. Hagiya Y, Fukuhara H, Matsumoto K, et al. Expression levels of PEPT1 and ABCG2 play key roles in 5-aminolevulinic acid (ALA)-induced tumor-specific protoporphyrin IX (PpIX) accumulation in bladder cancer. *Photodiagnosis Photodyn Ther*. 2013;10:288–295.
20. Matsumoto A, Matsui I, Katsuma Y, et al. Quantitative analyses of foot processes, mitochondria, and basement membranes by structured illumination. *Kidney Int Rep*. 2021;6:1923–1938.
21. Hama T, Nagesh PKB, Chowdhury P, et al. DNA damage is overcome by TRIP13 overexpression during cisplatin nephrotoxicity. *JCI Insight*. 2021;6:e139092.
22. Okushima H, Inoue K, Imai A, et al. Syntaxin 3 regulates apical membrane integrity in proximal tubule epithelial cells and prevents Fanconi syndrome development. *Kidney Int*. 2025;108:1088–1104.
23. Katsuma Y, Matsui I, Matsumoto A, et al. Endogenous activation of peroxisome proliferator-activated receptor-α in proximal tubule cells in counteracting phosphate toxicity. *Am J Physiol Renal Physiol*. 2024;327:F208–F223.
24. Feng D, Ngov C, Henley N, et al. Characterization of matricellular protein expression signatures in mechanistically diverse mouse models of kidney injury. *Sci Rep*. 2019;9:1–14.
25. Mori M, Gotoh S, Taketani S, et al. Hereditary cataract of the Nakano mouse: involvement of a hypomorphic mutation in the coproporphyrinogen oxidase gene. *Exp Eye Res*. 2013;112:45–50.
26. Droebner K, Pavkovic M, Grundmann M, et al. Direct blood pressure-independent anti-fibrotic effects by the selective nonsteroidal mineralocorticoid receptor antagonist finerenone in progressive models of kidney fibrosis. *Am J Nephrol*. 2021;52:588–601.
27. Woods JS. Regulation of porphyrin and heme metabolism in the kidney. *Semin Hematol*. 1988;25:336–348.
28. Belot A, Puy H, Hamza I, et al. Update on heme biosynthesis, tissue-specific regulation, heme transport, relation to iron metabolism and cellular energy. *Liver Int*. 2024;44:2235–2250.
29. Yamamoto M, Kure S, Engel JD, et al. Structure, turnover, and heme-mediated suppression of the level of mRNA encoding rat liver delta-aminolevulinate synthase. *J Biol Chem*. 1988;263:15973–15979.
30. Eriksen L, Eriksen N, Haavaldsen S. The formation of coproporphyrin III and I by rabbit reticulocytes under hypoxic conditions *in vitro*. *Acta Physiol Scand*. 1961;53:308–314.
31. Weng J, Wang Y, Zhang Y, et al. an activatable near-infrared fluorescence probe for *in vivo* imaging of acute kidney injury by targeting phosphatidylserine and caspase-3. *J Am Chem Soc*. 2021;143:18294–18304.
32. Wang B, Tang C, Lin E, et al. NIR-II fluorescence-guided liver cancer surgery by a small molecular HDAC6 targeting probe. *EBioMedicine*. 2023;98:104880.
33. Feng X, Wang G, Pan J, et al. Purification-free synthesis of bright lactoglobulin@dye nanoprobe for second near-infrared fluorescence imaging of kidney dysfunction *in vivo*. *Colloids Surf B Biointerfaces*. 2024;236:13796.
34. Ly A, Nivison-Smith L, Assaad N, et al. Fundus autofluorescence in age-related macular degeneration. *Optometry Vision Sci*. 2017;94:246–259.
35. Morgan ML, Kaushik DK, Stys PK, et al. Autofluorescence spectroscopy as a proxy for chronic white matter pathology. *Mult Scler*. 2021;27:1046–1056.
36. Li M, Zhang X, Zhou Y, et al. Near infrared-activatable biomimetic nanoplatform for tumor-specific drug release, penetration and chemo-photothermal synergistic therapy of orthotopic glioblastoma. *Int J Nanomed*. 2024;19:6999–7014.
37. Koning S, van Kersen J, Tange FP, et al. The impact of diabetes mellitus on foot perfusion measured by ICG NIR fluorescence imaging. *Diabetes Res Clin Pract*. 2024;214:111772.
38. Huang T-T, Chen K-C, Wong T-Y, et al. Two-channel autofluorescence analysis for oral cancer. *J Biomed Opt*. 2018;24:1–10.
39. Htun NM, Chen YC, Lim B, et al. Near-infrared autofluorescence induced by intraplaque hemorrhage and heme degradation as marker for high-risk atherosclerotic plaques. *Nat Commun*. 2017;8:75.